Journal of Alloys and Compounds 509 (2011) 9791–9797

Contents lists available at ScienceDirect

Journal of Alloys and Compounds

journal homepage: www.elsevier.com/locate/jallcom

The induced synthesis of mixed phase niobate by Cu doping and its photocatalytic property

Gaoke Zhang[a,*], Jie Gong[a,b], Huihui Gan[a], Fan Lü[a]

[a] School of Resources and Environmental Engineering, Wuhan University of Technology, 122 Luoshi Road, Wuhan 430070, PR China
[b] School of Resources and Environmental Engineering, Wuhan University of Science and Technology, Qingshan District, Wuhan 430081, PR China

ARTICLE INFO

Article history:
Received 22 May 2011
Received in revised form 10 July 2011
Accepted 30 July 2011
Available online 4 August 2011

Keywords:
Niobate
Potassium
Copper doping
Tungsten–bronze structure
Layered perovskite structure
Photocatalysis
Mixed phase
Acid red G

ABSTRACT

Cu-doped KNb_3O_8 photocatalysts were prepared using a simple solid-state method. The catalysts were characterized by X-ray diffraction (XRD), scanning electron microscopy (SEM), photoluminescence (PL), X-ray photoelectron spectroscopy (XPS) and UV–vis diffuse reflectance spectrum. XRD and SEM analyses suggest that Cu doping can induce the formation of the compound $K_6Nb_{10.8}O_{30}$ with tungsten–bronze structure and the relative content of $K_6Nb_{10.8}O_{30}$ in the Cu-doped samples increased with increasing Cu doping amount. When the Cu doping amount reaches 2 wt.%, the as-prepared sample is mainly composed of $K_6Nb_{10.8}O_{30}$. The photocatalytic properties of the catalysts were evaluated using the degradation of acid red G. The results showed that Cu-doping significantly increased the photocatalytic activity of the KNb_3O_8 catalyst. The optimum dopant concentration range of Cu was found to be 0.3–1 wt.%. The synergistic effect of Cu doping and mixed phase niobate compounds is responsible for the enhanced photocatalytic activity.

© 2011 Elsevier B.V. All rights reserved.

1. Introduction

Removal of color in wastewater from textile industries is an important problem to be resolved all over the world. Colored waters have a strong impact in the population and generate strong public complaints [1]. The release of these colored wastewaters in the ecosystem is a big source of aesthetic pollution, eutrophication and perturbations to aquatic life [2]. A variety of physical, chemical and biological methods are presently available for treatment of textile wastewater. Although biological treatment using activated sludge is an effective technology, it has been reported that the majority of dyes are only adsorbed on the sludge and are not degraded [3]. Physical methods such as ion-exchange, adsorption, etc., only simply transfer the pollutants to another phase rather than destroying them [4]. Photocatalytic methods, using semiconductors, such as TiO_2, have attracted extensive attention, because they provide a promising strategy for cleaning polluted air or water [5–7]. Some niobates, such as $K_4Nb_6O_{17}$ [8], Bi_2InNbO_7 [9], $Sr_2Nb_2O_7$ [10], Bi_3NbO_7 [11] have been attracting attention lately because they are much more active than the generally used TiO_2 for photocatalytic water splitting [12]. In an earlier study, we have found that KNb_3O_8 and $K_6Nb_{10.8}O_{30}$ have high photocatalytic activity against acid red G [13,14]. KNb_3O_8 contains octahedral [NbO_6] units forming an anionic sheet disposed in a stacking arrangement [15]. The charge balance is maintained by the presence of potassium ions between the layers. The KNb_3O_8 crystal was observed to be the layered structure of perovskite. The crystal structure of $K_6Nb_{10.8}O_{30}$ is constructed by NbO_6 octahedra, which form some triangle, quadrilateral and pentagonal tunnels. The pentagonal and quadrilateral tunnels are occupied by K cations and the triangle tunnels are occupied by Nb cations [16,17].

It is known that transition metal ions doped into the catalysts can increase the quantum efficiency of the heterogeneous photocatalytic property by acting as electron (or hole) traps and by altering the e^-/h^+ pair recombination rate [18–20]. In the past decades, doping of TiO_2 with transition metal ions was explored by many researchers to improve the photocatalytic properties of semiconductor nanoparticles [21,22]. Yanagisawa et al. [23] reported Cu^{2+} doped hydrogen tetratitanate could enhance the photocatalytic activity by constructing Pt and TiO_2 pillars in the interlayer. Chen et al. [24] found that the $Bi_2Zn_{2/3}Ta_{4/3}O_7$ with small amount of Cu doped showed a desirable photocatalytic activity under both ultraviolet and visible light irradiation. It is of great interest to investigate the influence of the Cu doping on the physico-chemical property and photocatalytic activity of KNb_3O_8. In the present

* Corresponding author. Tel.: +86 27 87651816; fax: +86 27 87887445.
E-mail addresses: gkzhang@whut.edu.cn, zgkwu@126.com (G. Zhang).

0925-8388/$ – see front matter © 2011 Elsevier B.V. All rights reserved.
doi:10.1016/j.jallcom.2011.07.108

paper, the compound KNb_3O_8 doped with Cu was prepared by the solid-state reaction method, and the photocatalytic properties of as-prepared samples were evaluated by the degradation of 50 mg/L acid red G solution over the catalysts under UV irradiation. The effect of Cu on the activity of the catalyst was also discussed.

2. Experimental

2.1. Preparation and characterization of samples

The Cu-doped KNb_3O_8 was prepared by solid-state reaction. Niobium pentoxide (Nb_2O_5, Shanghai Chemical Reagent Co., China), Copper Sulfate Pentahydrate ($CuSO_4{\cdot}5H_2O$, Henan Jiaozuo Chemical Second Factory, China) and potassium carbonate (K_2CO_3, Tianjin Chemical Reagent Factory, China) with analytical grade were selected as starting materials. Mixed raw materials with the stoichiometric proportion (Cu doping amount was calculated according to CuO content; considering complementing the volatilization of potassium, potassium carbonate was excessive 10%) were ground with an agate mortar for 30 min, sintered in an Al_2O_3 crucible at 900 °C for 2 h, then cooled to room temperature. The obtained samples were manually grinded again with the agate mortar.

XRD analysis of the as-prepared samples was carried out on a D/MAX-RB powder X-ray diffractometer (Rigaku, Japan) at 40 kV and 50 mA equipped with CuKα radiation (λ = 0.1540558 nm). The crystal morphology of the as-prepared samples was investigated by scanning electron microscopy (SEM) on a JSM-5610LV scanning electron microscope. The surface properties of the as-prepared samples were characterized by X-ray photoelectron spectroscopy (XPS) in a Thermo ESCALAB 250 system with a monochromatic AlKα source and a charge neutralizer; all the binding energies were referenced to the C 1s peak at 284.8 eV of the surface adventitious carbon. The absorption edge of the as-prepared samples was measured using a UV–vis spectrophotometer (UV2550), and $BaSO_4$ was used as the reflectance standard in a UV–vis diffuse reflectance experiment. The photoluminescence spectra of the as-prepared sample were recorded with a Perkin Elmer (LS 55) fluorescence spectrometer at room temperature using an excitation wavelength of 210 nm.

2.2. Photocatalytic activity measurement

The photocatalytic activity of the as-prepared samples was evaluated by the degradation of 50 mg/L azo dye acid red G solution over the catalysts under UV irradiation. The acid red G (MW = 505 nm) was industrial grade and used without further purification. The photodegradation of acid red G was carried out in a 500 mL Pyrex glass vessel with magnetic stirring at room temperature. Light source was a 20 W UV lamp (λ = 253.7 nm). Reaction suspension was prepared by adding certain amount of the as-prepared samples into a 150 mL of acid red G aqueous solution. Prior to irradiation, the suspensions were magnetically stirred for 15 min in the dark to establish adsorption/degradation equilibrium. The distance between the liquid surface and the light source was about 8 cm. The light intensity was 0.750 mW/cm^2 measured by using an UV radiometer. Analytical samples were drawn from the reaction suspensions after various reaction times and centrifuged at 2000 rpm for 40 min to separate the particles. The concentrations of aqueous acid red G were analysed by UV–vis spectroscopy (UV-751GD) at its maximum absorption wavelength of 505 nm.

3. Results and discussion

3.1. XRD patterns analysis

The XRD patterns of Cu-doped KNb_3O_8 powders were shown in Fig. 1. The results show that the samples doped with Cu consist of two phases of the compound KNb_3O_8 with layered perovskite structure and $K_6Nb_{10.8}O_{30}$ with tetragonal tungsten–bronze structure. The peaks of the compound KNb_3O_8 in the XRD patterns became sharper with increasing the amount of Cu doping and the intensity of these peaks markedly decreased when the amount of Cu doping was more than 1 wt.%. The peaks of the compound $K_6Nb_{10.8}O_{30}$ appeared in the Cu-doped samples and the intensity of these peaks increased with increasing of the Cu doping amount. It is worthy noting that Cu doping can induce the formation of the compound $K_6Nb_{10.8}O_{30}$ in K_2O–Nb_2O_5 binary system and this result is consistent with previous research result [25]. The relative content of $K_6Nb_{10.8}O_{30}$ in Cu-doped sample increased with increasing Cu doping amount. When the Cu doping amount was increased to 2 wt.%, the as-prepared sample is mainly composed of $K_6Nb_{10.8}O_{30}$.

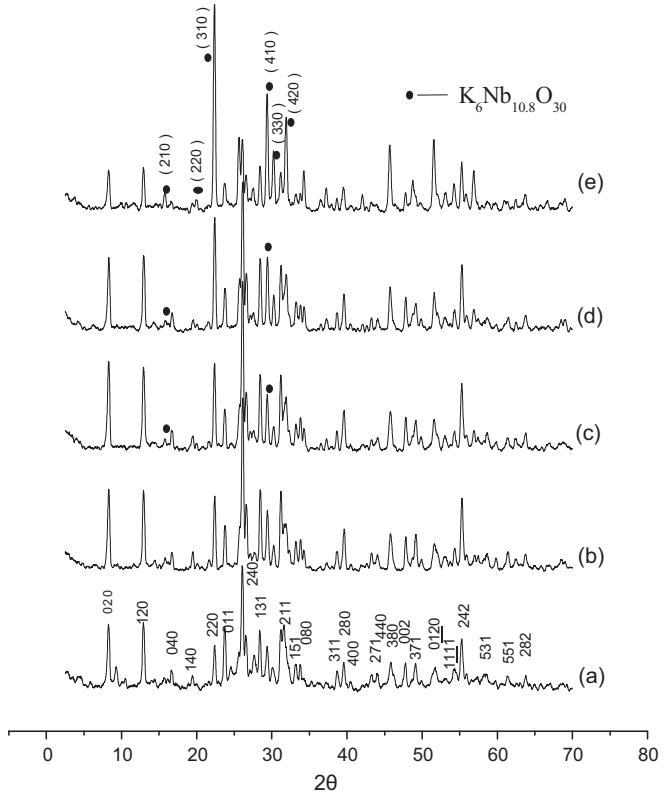

Fig. 1. XRD patterns of the prepared samples: (a) KNb_3O_8; (b) 0.3 wt.% Cu-doped; (c) 0.5 wt.% Cu-doped; (d) 1 wt.% Cu-doped and (e) 2 wt.% Cu-doped.

3.2. SEM analysis

Fig. 2 shows SEM images of the as-prepared samples un-doped and doped with Cu. Usually, the crystal morphology of KNb_3O_8 shows flake-like and the crystal of $K_6Nb_{10.8}O_{30}$ takes on quadrate column shape [13,14]. From Fig. 2, the crystal sizes increased and more and more uniform quadrate crystals formed with the increasing of the Cu doping amount. The result indicates that the Cu doping promotes the increasing of the crystal sizes and the uniform of the shape. Even more important, the result further confirms that the introduction of Cu can result in formation of mixed phase niobates ($K_6Nb_{10.8}O_{30}$ and KNb_3O_8), which is consistent with the result of XRD analysis.

3.3. XPS analysis

XPS analyses were performed to examine the niobium states on the surface of the as-prepared samples. The high resolution XPS spectra of the Nb3d region of the as-prepared catalyst are shown in Fig. 3. The Nb3d region is composed of Nb3d5/2 peak and Nb3d3/2 peak. From Fig. 3a, it can be seen that Nb in the pure KNb_3O_8 exists in Nb^{5+}. Fig. 3b indicates that the Nb3d region of the pure $K_6Nb_{10.8}O_{30}$ can be assigned to four peaks that result from the presence of Nb^{5+} in two different environments. The Nb3d region of the samples doped with 0.3 wt.%, 0.5 wt.% and 1 wt.% Cu can be assigned to six peaks that can be attributed to Nb in KNb_3O_8 and $K_6Nb_{10.8}O_{30}$. These results show that the samples doped with Cu is composed of mixed niobates, which is consistent with the results of XRD and SEM analysis. Usually, the Nb3d5/2 binding energy of the Nb^{5+} in niobate is 206.5–207.2 eV, The Nb3d5/2 binding energy of the Nb^{4+} in niobate is about 205.5 eV [26–28]. From Fig. 3e, the two main peaks are the Nb3d5/2 peak and Nb3d3/2 peak in $Nb^{5+}(1)O_6$ octahedra at binding energies of 206.6 and 209.3 eV. The higher binding energy

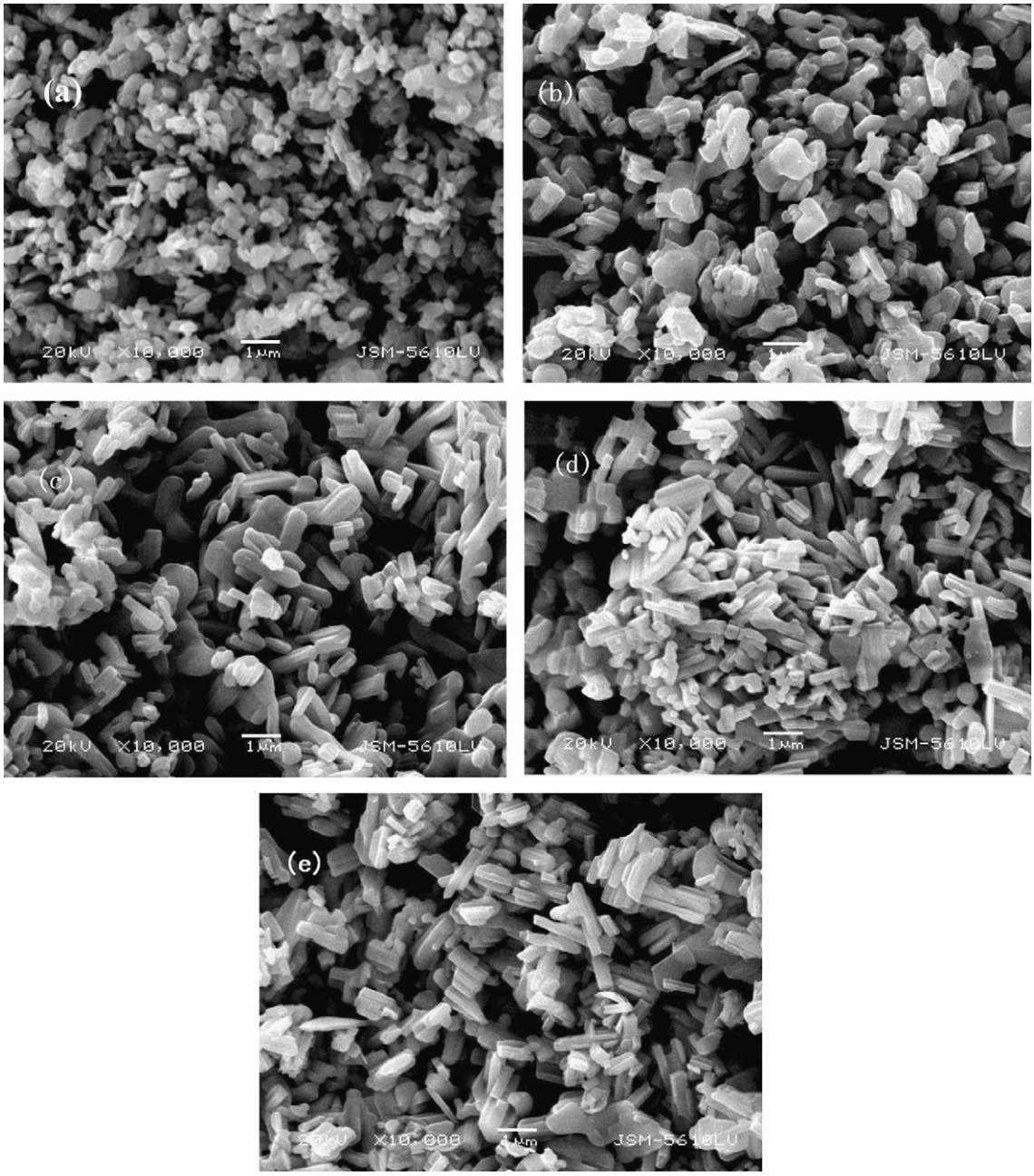

Fig. 2. SEM images of the as prepared samples: (a) KNb_3O_8; (b) 0.3 wt.% Cu-doped; (c) 0.5 wt.% Cu-doped; (d) 1 wt.% Cu-doped and (e) 2 wt.% Cu-doped.

peaks belong to the Nb3d5/2 peak and Nb3d3/2 peak of the $Nb^{5+}(2)$ in $Nb(2)O_6$ octahedra at binding energies of 207.5 and 210.7 eV. The lower binding energy peaks (206.2 and 209.1 eV) are attributed to the Nb3d5/2 peak and the Nb3d3/2 peak of the $Nb^{4+}(3)$ [29]. The results of XPS analysis reveal a small amount of Nb^{4+} may exist in the samples doped with 0.5 wt.% and 1 wt.% Cu [30]. The mixed valence and Cu-doping of niobium favor the photocatalytic activity of the catalyst through enhancing the distortion of the NbO_6 octahedra and the mobility of active oxygen in the crystal structure of the catalyst [25,31].

3.4. UV–vis diffuse reflectance spectrum analysis

The UV–vis diffuse reflectance spectra of KNb_3O_8, $K_6Nb_{10.8}O_{30}$ and KNb_3O_8 with different Cu doping amount are shown in Fig. 4. The absorption band at lower than 390 nm (ca. 3.18 eV) can be assigned to the intrinsic band gap absorption of the samples. As can be seen from Fig. 4, the pure KNb_3O_8 has an absorption edge at about 404.7 nm corresponding to the band gap energy of 3.06 eV, while the pure $K_6Nb_{10.8}O_{30}$ has an absorption edge at about 409.7 nm (ca. 3.03 eV). With increasing the Cu doping amount, on the one hand, the absorption characteristic of the Cu-doped KNb_3O_8 from 320 to 390 nm is gradually close to that of the pure $K_6Nb_{10.8}O_{30}$, which shows the ratio of the compound $K_6Nb_{10.8}O_{30}$ in the Cu-doped KNb_3O_8 sample gradually increases; this result is consistent with that of XRD and SEM analyses. On the other hand, the two absorption bands at about 420 nm and 600 nm appear in the Cu-doped KNb_3O_8 samples, which are related with the chemical environment of Cu in the structure of the Cu-doped niobate [25,32]. The absorption band at 420 nm may correspond to the charge transfer Cu–O–Nb, the band at 600 nm can be attributed to the d–d transition of Cu(II) ion in the octahedral sites [33–36]. From

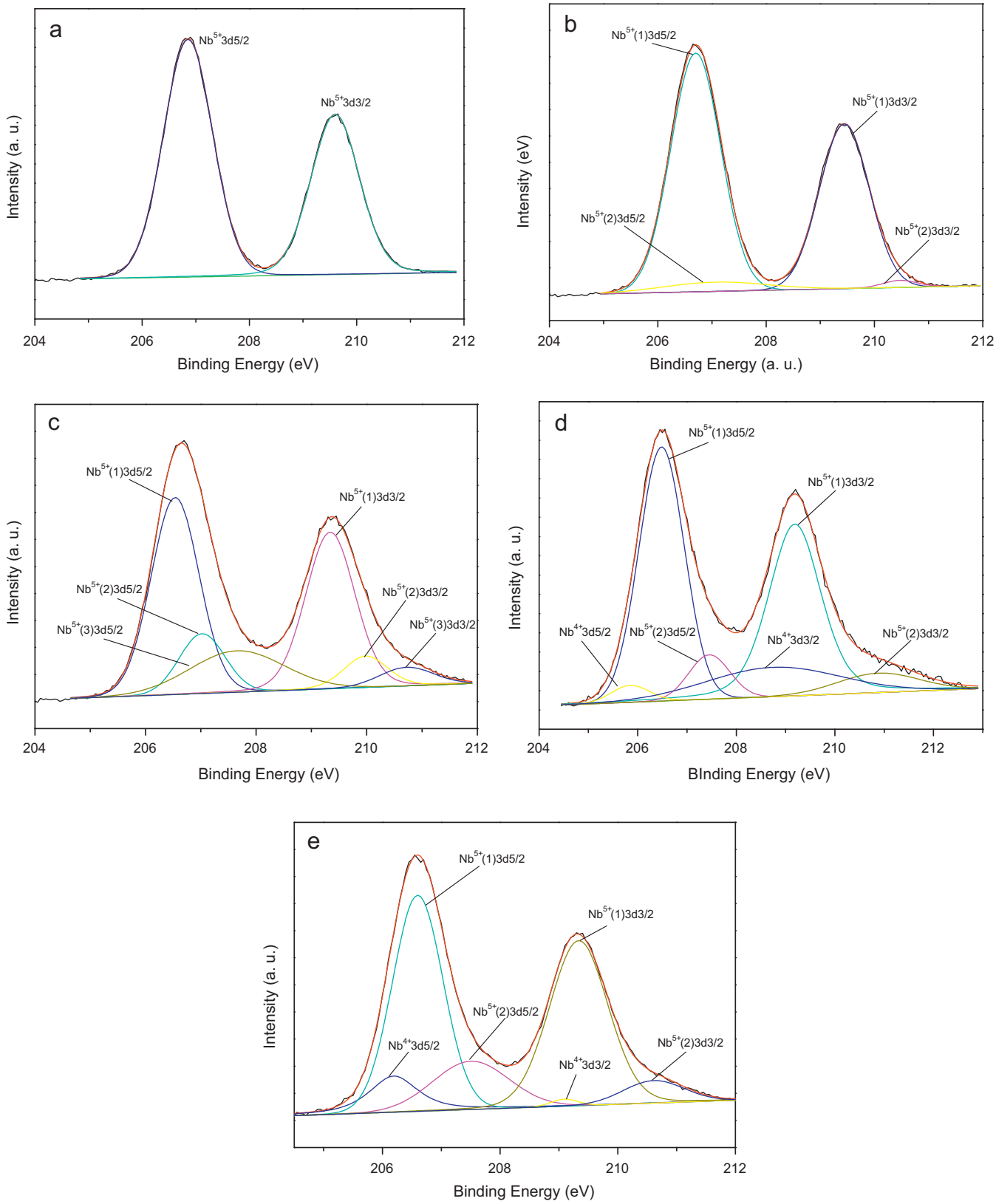

Fig. 3. High-resolution XPS spectra of the Nb3d region of the samples: (a) KNb_3O_8; (b) $K_6Nb_{10.8}O_{30}$; (c) 0.3 wt.% Cu-doped; (d) 0.5 wt.% Cu-doped and (e) 1 wt.% Cu-doped.

these results, Cu doping results in the formation of the compound $K_6Nb_{10.8}O_{30}$ in the Cu-doped KNb_3O_8 samples. The compound $K_6Nb_{10.8}O_{30}$ enhances the absorption of the Cu-doped KNb_3O_8 samples for UV light. Cu doptant increases the aborption of the Cu-doped KNb_3O_8 samples in visible light region and the red-shift of the absorption edge of the samples. To clarify the effect of the extended absorption wavelengths for Cu-doped KNb_3O_8, the photodegradation of acid red G using the Cu-doped KNb_3O_8

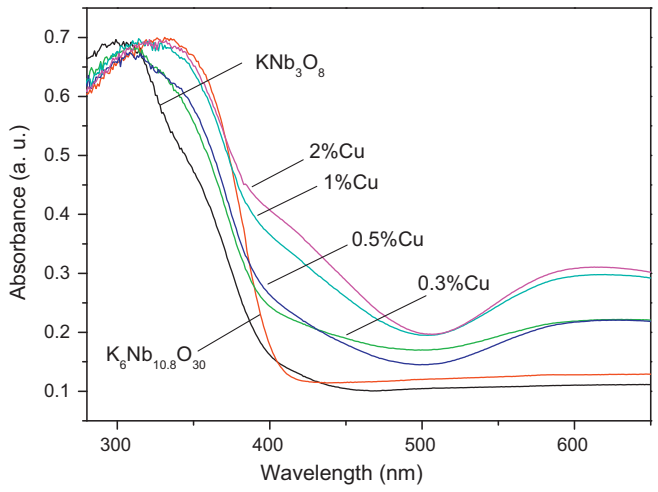

Fig. 4. The UV–vis diffuse reflectance spectra of KNb_3O_8, $K_6Nb_{10.8}O_{30}$ and Cu-doped KNb_3O_8 with different Cu doping concentration.

under visible light ($\lambda > 400$ nm) was performed. As a result, the photodecomposotion of acid red G was not confirmed under visible light irradiation for 2 h, suggesting that the optical absorption at wavelengths larger than 400 nm does not contribute to the visible light photocatalytic activity. Therefore, it may be plausible that Cu doping does not enhance the number of photoexcited carriers but extend their lifetime and increase the photogenerated electron mobility in the sample. This result is similar to that of Cu loaded $TiO_{2-x}N_x$ reported by Morikawa et al. [37].

3.5. Photocatalytic activity of the catalyst

The photocatalytic property of Cu-doped KNb_3O_8 was studied by the degradation of 50 mg/L acid red G. The dosage of catalyst was 1.0 g/L. As shown in Fig. 5a, the degradation rate of acid red G is very low under UV irradiation for 60 min without catalyst and in the presence of KNb_3O_8 catalyst in the dark respectively. Therefore, the presence of both UV illumination and photocatalyst is necessary for the efficient degradation of acid red G. Fig. 5 also shows the degradation rate of acid red G by KNb_3O_8 doped with different concentration Cu^{2+} as a function of UV irradiation time. After UV irradiation for 60 min, the photodegradation rate of acid red by the catalyst KNb_3O_8 was 63.03%. When using the catalysts KNb_3O_8 doped with 0.3 wt.%, 0.5 wt.%, 1 wt.% and 2 wt.% Cu, the photodegradation rates of acid red G after UV irradiating for 60 min could reach 93.23%, 93.06%, 93.63% and 83.92%, respectively, and which were higher than that of the pure KNb_3O_8. Via the first-order linear fit, the determined reaction rate constants, k, for the degradation of acid red G over the samples were shown in Fig. 5b. It is noted that doping with 0.3–1 wt.% Cu ions, which is the best dopant concentration range, can significantly increase the photocatalytic activity of KNb_3O_8 crystals. Fig. 6 displays UV–vis absorption spectra changes during the photodegradation reaction of acid red G by 0.3 wt.% Cu-doped KNb_3O_8. The UV–vis spectra for acid red G solution show three main absorption bands, the peak at 215 nm corresponded to the structure of benzene ring, the peak around 330 nm standard for the structure of naphthalene ring and the band at 505 nm correspondences to the nitrogen to nitrogen double bond (–N=N–), which was used to monitor the photodegradation of acid red G by catalyst, The decrease of the peaks of acid red G at 505 nm indicates a rapid degradation of azo dye and the –N=N– bond was destroyed, which is the most active site for oxidative attack in the structure of acid red G.

The Cu-doped KNb_3O_8 with the dopant concentration from 0.3 wt.% to 1 wt.% exhibit the excellent photocatalytic ability, while

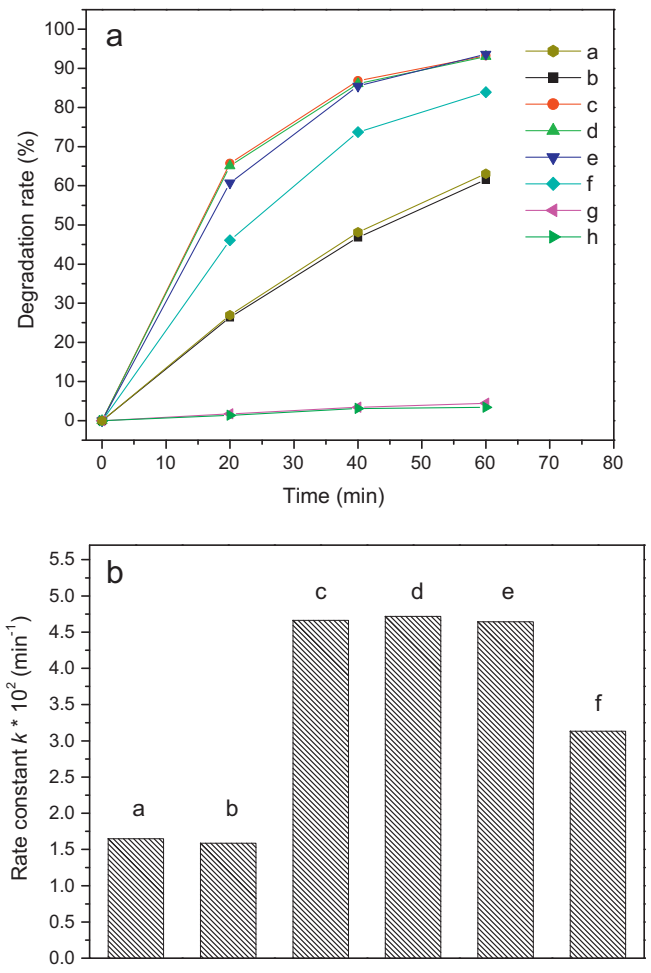

Fig. 5. The degradation rate of 50 mg/L acid red G under different conditions (a) and the comparison of rate constant k (b): (a) KNb_3O_8; (b) $K_6Nb_{10.8}O_{30}$; (c) 0.3 wt.% Cu doped KNb_3O_8; (d) 0.5 wt.% Cu doped KNb_3O_8; (e) 1 wt.% Cu doped KNb_3O_8; (f) 2 wt.% Cu doped KNb_3O_8; (g) in the absence of catalyst and (h) KNb_3O_8 catalyst in the dark.

with the further increase of the dopant concentration to 2 wt.%, the photocatalytic efficiency was decreased. Effects of Cu ions in aqueous media on the photodegradation of pollutants have been showed in some studies. Foster et al. [38] think the role of copper

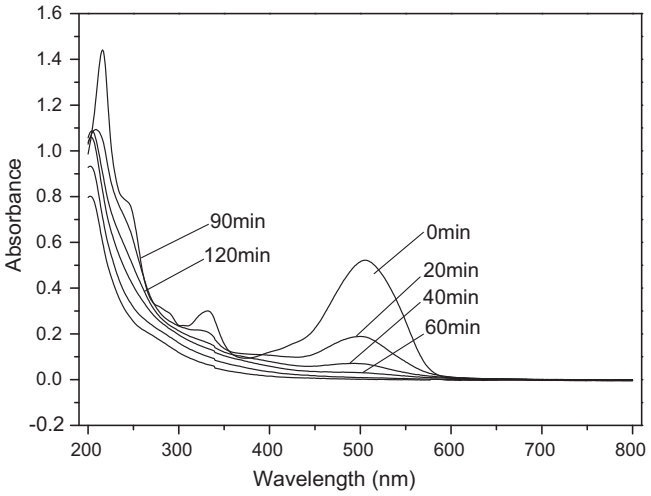

Fig. 6. Absorption changes during the photocatalytic degradation of 50 mg/L acid red G by 0.3 wt.% Cu-doped KNb_3O_8.

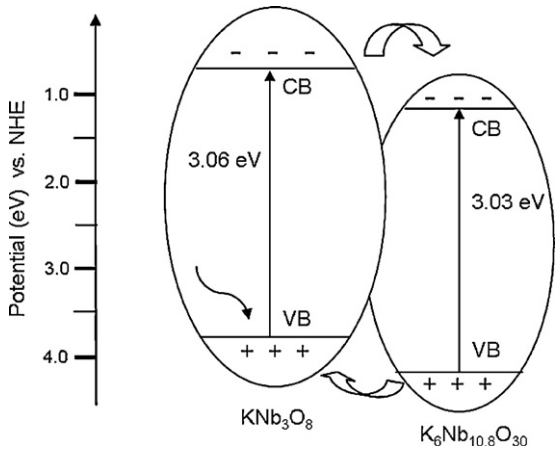

Fig. 7. Schematic diagram of the band energy levels of KNb_3O_8 and $K_6Nb_{10.8}O_{30}$ and the transfer procedure of photogenerated electrons and holes.

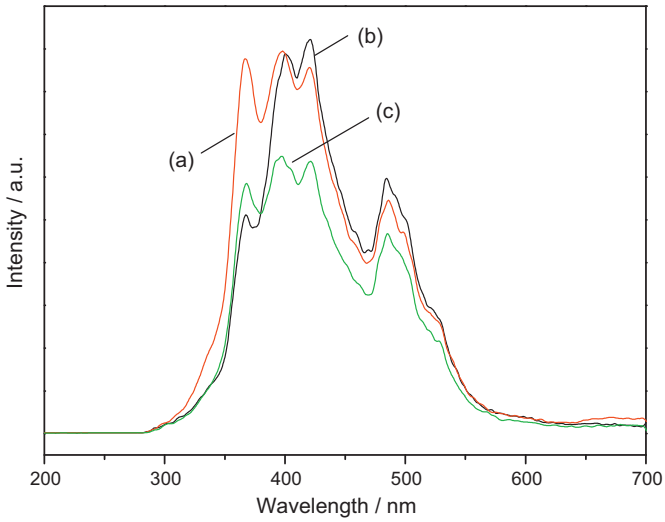

Fig. 8. Photoluminescence spectra of (a) KNb_3O_8; (b) $K_6Nb_{10.8}O_{30}$ and (c) 0.3 wt.% Cu-doped.

ions in solution in enhancing the photoactivity of titanium dioxide is generally believed to be via electron capturing at the semiconductor surface by the Cu(I) in it could be oxidized back to Cu(II). This has been said to prevent electron–hole recombination resulting in an increased rate of hydroxyl radicals' formation. Bideau and his coworkers [39,40] also have suggested the photocatalytic enhancement to occur through a redox cycle between adsorbed Cu(II) and Cu(I) on the surface of TiO_2. Beydoun et al. [41] pointed out that copper (II) ions readily form coordinated compounds. Such ternary complexes have been said to form between the copper ion, the organic or its oxidation intermediate, and an oxygen-containing species such as H_2O_2, O_2 of $O_2^{\bullet-}$. The ability of these compounds to take part in redox reactions, together with their photoreactivity have been said to be important for the photodegradation of organic pollutants in the environment. Sýkora [42] found that a catalytic effect of the Cu (II) ion occur either through redox Cu(II)–Cu(I) coupling reactions with the simultaneous the photodegradation of the pollutant present as a ligand in the coordination sphere of the copper central atom and/or be based on the secondary reactions of the active species produced photochemically from the copper complex. Cu doping can improve the photocatalytic property of Cu-doped $K_6Nb_{10.8}O_{30}$, but its photocatalytic activity markedly decreased when the amount of Cu doping above a certain level. The copper oxide at high loading was confined on the surface of catalysts and the trapped electrons were more apt to recombine with the holes.

Here, although Cu doping amount reaches 2 wt.%, KNb_3O_8 doped with Cu still shows higher photocatalytic activity than pure KNb_3O_8. This may be attributed to three reasons. Firstly, the layered materials use their interlayer space as reaction sites, where electron–hole recombination process could be retarded by physical separation of electron and hole pairs generated by photoabsorption. KNb_3O_8 belongs to layered perovskite compound, its photocatalytic activity is sensitive to its interlayer cations [43], Cu(II) ions can enter into the interlayer spaces [44], which may act as receptors or transmitters of photogenerated electrons so as to inhibit the recombination and extend the lifetime of charge carrier. Secondly, Cu doping can induce the formation of the compound $K_6Nb_{10.8}O_{30}$. The valence and conduction band edge (VB and CB) of KNb_3O_8 and $K_6Nb_{10.8}O_{30}$ at the point of zero charge can be calculated based on an atom's Mulliken electronegativity [45–47]. Accordingly, a scheme diagram of the band levels and charge-transfer procedure of KNb_3O_8 and $K_6Nb_{10.8}O_{30}$ is given in Fig. 7. Both the CB bottom and the VB top of $K_6Nb_{10.8}O_{30}$ lay below the CB bottom and VB top of KNb_3O_8, respectively. Under UV-light irradiation, an electron at the CB bottom of KNb_3O_8 would migrate to that of the $K_6Nb_{10.8}O_{30}$. Moreover, a hole at the VB top of the $K_6Nb_{10.8}O_{30}$ would migrate to that of KNb_3O_8. In this way, the formed nanostructure heterojunction on $K_6Nb_{10.8}O_{30}$ and KNb_3O_8 can lead to a more efficient interelectron transfer, which plays an important role for the enhanced photocatalytic activities. Thirdly, the highly distorted surface NbO_6 octahedral sites play an important role in heterogeneous catalysis. Cu(II) ions can enter into NbO_6 octahedral sites and increase the photocatalytic effect of the catalyst through enhancing the distortion of the NbO_6 octahedral and the mobility of active oxygen in the crystal structure of the catalyst. Nb with different environments and Nb^{4+} may be good for increasing the distortion of NbO_6 octahedra in the structure of the Cu-doped sample and improving its photocatalytic property.

To establish the above analysis, we measured the photoluminescence spectra of the photocatalysts, which is an effective way to study the efficiency of charge carrier trapping, immigration, transfer, as well as the surface oxygen vacancies and defects of semiconductor materials [48–50]. Fig. 8 shows the photoluminescence spectra of the pure KNb_3O_8, $K_6Nb_{10.8}O_{30}$ and the 0.3 wt.% Cu-doped KNb_3O_8. It can be seen that the samples exhibit a strong and wide PL signal at the range from 350 to 550 nm, having four obvious PL peaks at about 365, 395, 420 and 485 nm. The PL peak intensities of the 0.3 wt.% Cu doped KNb_3O_8 were largely decreased than that of the pure KNb_3O_8 and $K_6Nb_{10.8}O_{30}$, indicating that the recombination of photogenerated charge carrier was inhibited greatly in the 0.3 wt.% Cu doped KNb_3O_8. The photo-induced electrons in the Cu doped KNb_3O_8 can easily transfer, which promotes the separation of the electron–hole pairs, resulting in the increase of photocatalytic activity. This result shows good agreement with that of Fig. 6 and analysis above.

4. Conclusion

Cu doped KNb_3O_8 catalysts were prepared by a solid-state method, and their photocatalytic properties were investigated. A significant enhancement of the photocatalytic property was attainable by Cu doping. Cu doping could induce the formation of the compound $K_6Nb_{10.8}O_{30}$. The ratio of $K_6Nb_{10.8}O_{30}$ in Cu-doped sample increased with increasing Cu doping amount. XPS analysis confirmed that the niobium with mixed valence state existed in the Cu doped KNb_3O_8 catalysts. Cu doping resulted in a red shift of the photophysical response of the compound KNb_3O_8 and increased the adsorption of the Cu-doped KNb_3O_8 samples in the visible light region. The Cu doping, mixed valence of niobium and the formed

heterojunction on mixed niobates could be conducive to enhance photocatalytic activity.

Acknowledgements

This work was supported by the National Natural Science Foundation of China (50872103), National Basic Research Program of China (973 Program) 2007CB613306 and the Project-sponsored by SRF for ROCS, SEM.

References

[1] C.G. da Silva, J.L. Faria, J. Photochem. Photobiol. A. 155 (2003) 133–143.
[2] J.M. Herrmann, M. Vautier, C. Guillard, J. Catal. 201 (2001) 46–59.
[3] U. Pagga, K. Taeger, Water Res. 28 (1994) 1051–1057.
[4] G. Cesconeto Neto, H.J. José, R.F.P.M. Moreira, J. Photochem. Photobiol. A 149 (2002) 147–154.
[5] X.W. Zeng, Y.X. Gan, E. Clark, L.S. Su, J. Alloys Compd. 509 (2011) L221–L227.
[6] K.L. Lv, J.G. Yu, L.Z. Cui, S.L. Chen, M. Li, J. Alloys Compd. 509 (2011) 4557–4562.
[7] N. Wang, X.Y. Li, Y.X. Wang, X. Quan, G.H. Chen, Chem. Eng. J. 146 (2009) 30–35.
[8] S. Uchida, Y. Fujishiro, A. Watanabe, O. Ito, T. Sato, J. Chem. Soc., Dalton Trans. 93 (1997) 3229.
[9] Z. Zou, J.H. Ye, H. Arakawa, Chem. Mater. 13 (2001) 1765–1769.
[10] G.K. Hyun, W.H. Dong, K. Jindo, G.K. Young, S.L. Jae, Chem. Commun. 107 (1999) 7–1078.
[11] G.K. Zhang, J.L. Yang, S.M. Zhang, Q. Xiong, B.B. Huang, W.Q. Gong, J. Hazard. Mater. 172 (2009) 986–992.
[12] W.F. Yao, H. Wang, X.H. Xu, S.X. Shang, Y. Hou, Y. Zhang, M. Wang, Mater. Lett. 57 (2003) 1899–1902.
[13] G.K. Zhang, J. Gong, X. Zou, F.S. He, H. Zhang, Q. Zhang, Y. Liu, X. Yang, B. Hu, Chem. Eng. J. 123 (2006) 59–64.
[14] G.K. Zhang, X. Zou, J. Gong, F.S. He, H. Zhang, Q. Zhang, Y. Liu, X. Yang, B. Hu, J. Alloys Compd. 425 (2006) 76–80.
[15] M. Gasperin, Acta Cryst. B 38 (1982) 2024–2026.
[16] P. Becker, P. Held, Z. Kristallogr. NCS 215 (2000) 319.
[17] M. Lundberg, M. Sundberg, J. Solid State Chem. 63 (1986) 216–230.
[18] M. Gratzel, R.F. Howe, J. Phys. Chem. 94 (1990) 2566–2572.
[19] X.H. Xia, Y. Gao, Z. Wang, Z.J. Jia, J. Phys. Chem. Solids 69 (2008) 2888–2893.
[20] R.M. Mohamed, I.A. Mkhalid, J. Alloys Compd. 501 (2010) 301–306.
[21] S.C. Martin, C.L. Morrison, M.R. Hoffmann, J. Phys. Chem. 98 (1994) 13695.
[22] B.Z. Tian, J.L. Zhang, T.Z. Tong, F. Chen, Appl. Catal B. 79 (2008) 394–401.
[23] M. Yanagisawa, S. Uchida, T. Sato, Int. J. Inorg. Mater. 2 (2000) 339–346.
[24] J.X. Sun, G. Chen, Y.X. Li, C. Zhou, H.J. Zhang, J. Alloys Compd. 509 (2011) 1133–1137.
[25] G.K. Zhang, X. Zou, J. Gong, F.S. He, H. Zhang, S.X. Ouyang, H.X. Liu, Q. Zhang, Y. Liu, X. Yang, B. Hu, J. Mol. Catal. A: Chem. 255 (2006) 109–116.
[26] K. Tabata, T. Choso, Y. Nagasawa, Surf. Sci. 408 (1998) 137–145.
[27] K. Tabata, M. Kamada, T. Choso, H. Munakata, Appl. Surf. Sci. 125 (1998) 93–98.
[28] V.V. Atuchina, I.E. Kalabin, V.G. Kesler, N.V. Pervukhina, J. Electron Spectrosc. Relat. Phenom. 142 (2005) 129–134.
[29] N. Kumadal, N. Kinamura, Eur. J. Solid State Inorg. Chem. 34 (1997) 65.
[30] G.K. Zhang, Y.J. Hu, X.M. Ding, J. Zhou, J.W. Xie, J. Solid State Chem. 181 (2008) 2133–2138.
[31] M. Ziolek, Catal. Today 78 (2003) 47–64.
[32] G.K. Zhang, L.Q. Qin, Mater. Chem. Phys. 74 (2002) 324–327.
[33] O.V. Komova, A.V. Simakov, V.A. Rogov, D.I. Kochubei, G.V. Odegova, V.V. Kriventsov, E.A. Paukshtis, V.A. Ushakov, N.N. Sazonova, T.A. Nikoro, J. Mol. Catal. A: Chem. 161 (2000) 191–204.
[34] H.L. Tang, Y. Ren, B. Yue, S.R. Yan, H.Y. He, J. Mol. Catal. A: Chem. 260 (2006) 121–127.
[35] S. Velu, L. Wang, M. Okazaki, K. Suzuki, S. Tomura, Microporous Mesoporous Mater. 54 (2002) 113–126.
[36] R. Ben Achma, A. Ghorbel, S. Sayadi, A. Dafinov, F. Medina, J. Phys. Chem. Solids 69 (2008) 1116–1120.
[37] T. Morikawa, Y. Irokawa, T. Ohwaki, Appl. Catal. A. 314 (2006) 123–127.
[38] N. Foster, R. Noble, C. Koval, Environ. Sci. Technol. 27 (1993) 350–356.
[39] M. Bideau, B. Claudel, L. Faure, M. Rachimoellah, Chem. Eng. Commun. 93 (1990) 167–179.
[40] M. Bideau, B. Claudel, L. Faure, H. Kazouan, J. Photochem. Photobiol. A: Chem. 67 (1992) 337–348.
[41] D. Beydoun, H. Tse, R. Amal, G. Low, S. McEvoy, J. Mol. Catal. A: Chem. 177 (2002) 265–272.
[42] J. Sýkora, Coordinat. Chem. Rev 159 (1997) 95–108.
[43] M. Machida, K. Miyazaki, S. Matsushima, M. Arai, J. Mater. Chem. 13 (2003) 1433–1437.
[44] L.M. Nunes, A.G. de Souza, R.F. de Farias, J. Alloys Compd. 319 (2001) 94–99.
[45] M.C. Long, W.M. Cai, J. Cai, B.X. Zhou, X.Y. Chai, Y.H. Wu, J. Phys. Chem. B 110 (2006) 20211–20216.
[46] M.A. Butler, D.S. Ginley, J. Electrochem. Soc. 125 (1978) 228.
[47] Y. Xu, M.A.A. Schoonen, Am. Mineral. 85 (2000) 543–556.
[48] J.J. Xu, Y.H. Ao, D.G. Fu, C.W. Yuan, Appl. Surf. Sci. 254 (2008) 3033–3038.
[49] J.K. Zhou, M. Takeuchi, A.K. Ray, M. Anpo, X.S. Zhao, J. Colloid Interface Sci. 311 (2007) 497–501.
[50] X.Y. Li, Y. Hou, Q.D. Zhao, G.H. Chen, Langmuir 27 (2011) 3113–3120.